Military Technical College
Kobry El-Kobba
Cairo, Egypt

12-th International Conference
on
Aerospace Sciences &
Aviation Technology

EXPERIMENTAL DETERMINATION OF GYRO DYNAMIC PARAMETERS OF A TYPICAL IR-SEEKER

ALI* M.S. and ALI* A.A.

ABSTRACT

The experimental identification of the dynamic parameters of the IR-seeker gyroscope is essential for the evaluation of the relative magnitudes of the different dynamic error sources and the seeker tracking capability.The gyroscope dynamic parameters include cross-axis spring rate, viscous damping coefficient of rotor about spin axis, magnetic torque damping, pendulous unbalance along spin axis, direct axis spring rate, and the mechanical viscous damping.The response of the system was measured experimentally due to a given finite input. The amplitude of the precession torque due to control current was determined. The numerical solution, of the seeker dynamic equations, is introduced based on the values of the parameters that are experimentally determined. The numerical results are compared with the experimental results for different conditions. The results of the numerical solution with changing the modeling parameters are introduced to predict the system response in each case.

KEY WORDS

Gyroscope, Gyro, IR-Seeker, Dynamical parameters, Cross-axis.

*Egyptian Armed Forces

NOMENCLATURE

A_{cage}	Cage coil signal amplitude [V]
A_{ref}	Reference sinusoidal signal amplitude [V]
a_x, a_y, a_z	Vehicle acceleration components projected into the vehicle coordinate system [m/s^2]
D	Viscous damping about the gimbal axes, or mechanical viscous damping in [N.m/rad/s]
D_r	Viscous drag on the rotor about its spin axis, or viscous damping coefficient of rotor about spin axis [N.m/rad/s]
d	Horizontal distance between the infrared source and the origin of the board coordinate system [m]
E_1	Line-of-sight error in yaw
E_2	Line-of-sight error in pitch
f	Angular frequency of the reference signal [Hz]
G1, G2, G3	Amplifier gains and Integrator gain
g	Gravity field [m/s^2]
H	Angular momentum of the spinning rotor [kg.m^2.rad/s]
K	Mechanical spring rate about the gimbal axes or the direct-axis spring rate in [N.m/rad]
L	Distance between the infrared source at the origin of the board coordinate system and the center of support of gyro gimbals [m]
p	Fixed pendulous unbalance along spin axis [Kg.m]
t	Time [s]
V_{cage}	The cage coil signal after amplification
V_{cage0}	Cage coil signal [V]
$V_{o/p}$	DC output voltage proportional to the seeker look angle in pitch [V]
$V_{o/y}$	DC output voltage proportional to the seeker look angle in yaw [V]
$V_{ref\,0}$	Reference sinusoidal signal [V]
$V_{ref.\sin.}$	The reference sinusoidal signal after amplification
$V_{ref.\cos.}$	The integrated cosine signal
α	Angular misalignment of the detector head with respect to the spinning-axis (s-axis) [rad]
δT_p	Magnetic torque damping in [N.m/rad/s]
ϕ	Yaw angle [rad]
φ_{cage}	Cage coil signal phase shift [rad]
$\lceil \dot{\gamma} \rceil$	Angular velocity of the vehicle w.r.t the frame of fixed orientation [rad/s]
$\lceil \ddot{\gamma} \rceil$	Angular acceleration of the vehicle w.r.t the frame of fixed orientation [rad/s^2]
θ	Pitch angle [rad]
ω_r	Spinning angular velocity of the rotor, angular frequency of the reference signal [rad/s]

1. INTRODUCTION

The problem of obtaining perfect and accurate stabilized elements represents the main problem in the design [1, 2] of high performance inertial navigation and guidance systems [3]. The accuracy and performance of these systems depend strongly and mainly on the accuracy and the perfect stabilization of these stabilized elements, which must be isolated from the local angular motion of their transporting vehicle. The investigation of these elements stability should be based upon the known properties of gyroscopes, the reason that gives special interest to the gyros dynamic and its configurations [4, 5]. The gyro-stabilized solenoidal-torqued seeker [6] is the most common structure in a several low cost gyro-stabilized seekers assemblies for missiles guidance and tracking applications. The availability of references that discuss the seeker dynamic equations of motion and introduce practical steps for the experimental determination of the dynamic parameters are rather limited in the open literature. The knowledge of these dynamic parameters is extremely important to study the effect of the modeling parameters on the system response and the evaluation of the seeker tracking capability.

The dynamic equations of motion of the gyroscope used inside a gyro-stabilized magnetic torqued seeker are derived [7-9] and its numerical solution is calculated. The dynamic parameters employed in that numerical solution are obtained through experimental investigations conducted on the gyro. The gyroscope dynamic parameters include rotor-response time constant due to cross-axis spring coupling, spin motor torque, direct axis spring rates, magnetic torque damping, and the pendulous unbalance along spin axis. A Computer simulation for the equations of motion is illustrated. The effects of the modeling parameters on the system response are investigated. The prediction of the system response based on real values of the equations parameters can be considered as an essential step to any future development in the seeker system, which can be modified or reconstructed using more advanced techniques.

2. GYRO EQUATIONS OF MOTION

The dynamic equations of motion of the gyro-mass of the gyro-stabilized magnetic torqued seeker are derived [9] and can be reducing to a simplified form according to the following assumptions:

i) To eliminate cross-axis terms in the equations, by design set

$I_s = I_a = I_b = I$

ii) The seeker head will be operating within a narrow cone; therefore, the use of small-angle approximations appears justified.

$\cos\theta = 1 \qquad \sin\theta = \theta \qquad \cos\phi = 1 \qquad \sin\phi = \phi$

iii) Due to the small change in the spinning angular velocity of the rotor (ω_r), the rotor speed will be considered as essentially constant and the equation for the spin-axis dynamics will be dropped.

iv) linearize all dynamics not multiplied by $\dot{H}$ (rate of change of angular momentum). Now, the equations are reduce to

$$\alpha T_P E_1 - T_P E_2 - \phi T_{M1} - D_1\dot{\theta} - K\theta - (a_x\theta + a_z)p = I(\ddot{\gamma}_y + \ddot{\theta}) + H(\dot{\gamma}_x\theta + \dot{\gamma}_z + \dot{\phi}) \quad (1a)$$

$$T_P E_1 + \alpha T_P E_2 + \theta T_{M1} - D_1\dot{\phi} - K\phi - (a_x\phi - a_y)p = I(\ddot{\gamma}_z + \ddot{\phi}) - H(-\dot{\gamma}_x\phi + \dot{\gamma}_y + \dot{\theta}) \quad (1b)$$

Where

$$D_1 = D + \delta T p \quad (2)$$

$$T_{M1} = T_M + \delta T_P \omega_r \quad (3)$$

3. DETERMINATION OF THE GYRO-ROTOR LOOK ANGLE

The experimental determination of the gyro dynamic parameters is mainly based on measuring the gyro-rotor look angle versus time in the pitch and yaw planes using certain prearranged set-up. Due to the mechanical structure [10] of the IR-seeker gyroscope (homing head), the direct measurement of the gyro look angle was not possible. So, an indirect method is proposed for measuring this angle. This method depends on the linear relation between the look angle and the caging coil output voltage to produce a gyro rotor precession angle calibration curve. The look angle is considered as the tracked target angle (perfect tracking loop is considered).This calibration curve is used to transform the recorded cage coil output voltage to the corresponding rotor angles. The first step for making the calibration curve which is the offset and reference frame adjustment. It can be achieved by instantaneously monitoring the signal during gyro operation. It is a suitable method for real time measuring and testing (on-line reading). Also, the offset and reference frame adjustment can be made by an offline method for processing the data after gyro turn-off using data acquisitions card with a graphical user interface (GUI) software . Although this method is more accurate for measuring and testing, several trails are needed (off line method for data processing). Using the two methods respectively may ensure the accuracy without several trials.

3.1 Offset and Reference Frame Initial Adjustment

Fig.1 shows the schematic diagram of the test rig, and the experimental setup devices that are used in this process. Different signals are extracted from the gripstok plug and introduced to measuring devices. Fig.2 shows the real output signals; the reference signal which has a periodic waveform with constant amplitude and frequency. The cage coil signal has a sinusoidal waveform with constant frequency but its amplitude and phase are proportional to the seeker look-angle (magnitude and direction). It is noted that its phase is defined relative to the phase of the reference signal. Since the cage coil signal generally includes the yaw and pitch signal components. It is necessary to precess the gyro rotor in one plane only and recording the corresponding output signal. The reference coil location defines the pitch and yaw precession directions. The process shown in Fig.3 is followed to separate yaw and pitch components from the cage coil signal.

The cage coil signal

$$V_{cage\,0} = A_{cage}\sin(\omega_r t + \varphi_{cage}) \quad (4)$$

Where

ω_r is the angular frequency of the reference signal

is amplified [11] using the amplifier (1), with gain $G_1 = 11$. The average DC level of the cage coil signal before amplification is 0.15 volt/ degree. The cage coil signal after amplification will be:

$$V_{cage} = G_1 A_{cage} \sin(\omega_r t + \varphi_{cage}) \tag{5}$$

While the reference sinusoidal signal

$$V_{ref\,0} = A_{ref} \sin \omega_r t \tag{6}$$

is amplified using the amplifier (2), with gain $G_2 = 6$. The amplitude of the reference signal before amplification is 5 volt p/p. The reference sinusoidal signal after amplification will be:

$$V_{ref.\sin.} = G_2 A_{ref} \sin \omega_r t \tag{7}$$

The amplified reference sinusoidal signal (sin) is integrated using integrator circuit [11] to a cosine signal (cos). The integrated cosine signal is given by:

$$V_{ref.\cos.} = -G_3 G_2 A_{ref} \cos \omega_r t \tag{8}$$

Where G_3 is the integrator gain:

$$G_3 = -\frac{R_5}{R_4} \tag{9}$$

R_4 is a variable resistance tuned to obtain equal amplitude of the output (reference cosine) and the input (reference sine) of the integrator circuit.

The analog multipliers of the analog computer is used to resolve the polar cage coil signal into pitch and yaw signals separated as shown in Fig.3. The inputs to the analog computer are:

The cage coil signal, $V_{cage} = G_1 A_{cage} \sin(\omega_r t + \varphi_{cage})$, and

the reference sine signal, $V_{ref.\sin.} = G_2 A_{ref} \sin \omega_r t$, and

the integrated reference cosine signal, $V_{ref.\cos.} = -G_2 A_{ref} \cos \omega_r t$.

The outputs from the analog computer are two separated AC signals:

$$\begin{aligned} V_{cage/p} &= -G_1 G_2 A_{cage} A_{ref} \sin(\omega_r t + \varphi_{cage}) \cos \omega_r t \\ &= \frac{-G_1 G_2 A_{cage} A_{ref}}{2} \left[\sin\left(2\omega_r t + \varphi_{cage}\right) + \sin\left(\varphi_{cage}\right)\right] \end{aligned} \tag{10a}$$

$$\begin{aligned} V_{cage/y} &= G_1 G_2 A_{cage} A_{ref} \sin(\omega_r t + \varphi_{cage}) \sin \omega_r t \\ &= \frac{G_1 G_2 A_{cage} A_{ref}}{2} \left[\cos\left(\varphi_{cage}\right) - \cos\left(2\omega_r t + \varphi_{cage}\right)\right] \end{aligned} \tag{10b}$$

These are the look-angle components in pitch and yaw. Its DC-offset is proportional to the seeker look-angle in pitch and yaw, respectively. These outputs are introduced to low pass filters (LPF) circuit [11] to remove the AC component and keep only the DC level to yield DC output voltages:

$$V_{o/p} = -\frac{1}{2} G_1 G_2 A_{cage} A_{ref} \sin(\varphi_{cage}) \tag{11a}$$

$$V_{o/y} = \frac{1}{2} G_1 G_2 A_{cage} A_{ref} \cos(\varphi_{cage}) \tag{11b}$$

These outputs are proportional to the seeker look angle in pitch and yaw, respectively.

To produce the cage coil signal, an infrared source is mounted on a movable carrier which can be displaced on a vertical plane board placed in front of the seeker dome at a distance 286 cm from the center of support (CS) of the gyro gimbals. The board is divided into equal vertical and horizontal cells of 5 cm side. When the infrared source is moved and the homing head is placed in the track mode, the separated DC voltages $V_{o/p}$ and $V_{o/y}$ are changed. Thus, they are recorded at the end of each cell (i.e. with step 5 cm). It is assumed that the homing head is an ideal tracker, i.e. the look angle of the gyro rotor equals to the target angle relative to the head axis.

The offset is adjusted by moving the infrared source in horizontal and vertical direction until a zero output voltages $V_{o/p}$ and $V_{o/y}$ are obtained. The position of the zero offset is considered to be the origin of the board coordinate system (O_T).

To adjust the missile body coordinate system with the board coordinate (ground coordinate) system the missile frame is rolled around its longitudinal axis until we obtain a zero $V_{o/p}$ value, which will remain zero while moving the infrared source horizontally.

3.2 Offset and Reference Frame Fine Adjustment

A data acquisitions card is used with a graphical user interface (GUI) software to process the signals. Fig.4 shows the schematic diagram of the test rig, the missile system, and the experimental setup devices, which are used in this process. The process shown in Fig.5 is performed to separate yaw and pitch components from the cage coil signal. The reference signal and the cage coil signal are collected. The DC levels are removed by subtracting the average value of each data array. Higher frequency noises are removed using Matlab [12, 13] low-pass filter as shown in Fig.6. The Matlab/ Simulink derivative is used to generate a cosine signal (cos.) from the reference sinusoidal signal (sin.). The Matlab/ Simulink multipliers are used to resolve the polar cage coil signal into pitch and yaw separate signals as shown in Fig.5. The inputs to the multipliers are; the cage coil signal, the reference sine signal, and the cosine signal, Fig7a. The outputs from the multipliers are two separated AC signals; $V_{cage/p}$ and $V_{cage/y}$. These are proportional to the look-angle components in pitch and yaw, Fig7b. Its DC-offset are proportional to the seeker look-angle in pitch and yaw, respectively. The separated DC voltages $V_{o/p}$ and $V_{o/y}$, Fig7c, remain constants and draw an approximately straight line in case of fixed seeker look-angle in pitch and yaw. The offset is adjusted and the missile body coordinate system is adjusted with the board coordinate (ground coordinate) system.

3.3 Calibration of DC Output Voltages against Seeker Look Angle

To represent the output DC voltages $V_{o/p}$ and $V_{o/y}$ as a function of look angle in degrees, the calibration procedure should be performed to obtain the relation between $V_{o/p}$ and $V_{o/y}$ and the look angle in pitch θ and yaw ϕ, respectively. The distance between the infrared source at the origin O_T and the center of support (CS)

of gyro gimbals is L = 286 cm. The infrared source is moved horizontally and the corresponding voltage $V_{o/y}$ is measured at the end of each cell (every 5 cm). The horizontal distance between the infrared source and the origin O_T is d.
The following relation gives the yaw angle

$$\phi = tan^{-1}\frac{d}{L} \tag{12}$$

The results are collected in the calibration curve in yaw direction, Fig.8. The variation in the shape of the $V_{o/y}$ curve between the positive and negative portion of yaw angle (phi) is due to the test reference coil which oriented along the pitch axis. The missile is rolled 90-degree counter clockwise. The test reference coil became perpendicular to its prior position to cancel its effect. The results are collected in the calibration curve in yaw direction, Fig.9, which insures the expected symmetrical behavior of $V_{o/y}$ against yaw angle. Position two is considered the best orientation of the missile system to minimize the effect of the test reference coil to obtain the normal operation behavior of the cage coil components in pitch and yaw.

Finally, the seeker look-angle in pitch (θ) and yaw (ϕ), which is used in the gyro torque equations, can be determined at different time intervals using the cage coil output signal. Also the derivatives $\dot{\theta}, \ddot{\theta}, \dot{\phi}$, and can be obtained using the Matlab program after smoothing the $\theta = \theta(t)$, $\phi = \phi(t)$ curves using poly fit module.

4. DETERMINATION OF THE ROTOR-RESPONSE DUE TO THE CROSS-AXIS SPRING COUPLING AND THE PENDULOSITY

The cross-axis spring rate (T_M), which is also the spin motor torque constant, can be measured by the time constant of the open-loop rotor response to an initial offset, e.g. an initial condition in either ϕ or θ with zero body rates. The system considered in the experimental work is a short-range missile [10]. A schematic diagram of the test rig, and the experimental setup devices that are used are shown in Fig.4. The infrared source is displaced horizontally a distance (d), the corresponding initial yaw angle is ϕ_0 . The pitch angle (θ) remains zero while moving the infrared source horizontally. The face of the seeker was masked and the values of the yaw and pitch angles were recorded. It is noticed that after the masking instant, the gyro rotor starts drifting [14, 15]. A polynomial fitting of the ϕ curve after masking instant is shown in Fig.10.There is no error (detector) signal reached to the precession amplifier when the seeker face was masked and the precession torque was vanished. The test conditions are summarized as follow:

a) $\dot{\gamma}_x = \dot{\gamma}_y = \dot{\gamma}_z = a_x = a_y = 0$

b) $T_p = 0$

c) $a_z = -g$

d) $\theta = 0$, $\dot{\theta} = 0$ and $\ddot{\theta} \approx 0$

Substitute these conditions into equation (1a), it results in:

$$pg - T_{M1}\phi = H\dot{\phi} \tag{13}$$

For any two successive equal time increments t_1 and t_2 equation (13) one can get:

$$T_{M1} = H\frac{(\dot{\phi}_1 - \dot{\phi}_2)}{(\phi_2 - \phi_1)} \tag{14}$$

Substituting ϕ, and $\dot{\phi}$ values into equation (14) at time t_1 and t_2, It results in $T_{M1}(average) = .00089\ N.m/rad$. Data can be taken for a positive and negative displacement of the infrared source on both the pitch and yaw direction separately. The test was repeated and the average value of T_{M1} was calculated.

The test was repeated with the precession coils opened to determine T_M ,Fig.11. where, the cross-axis spring rate due to induced current in precession coils ($\delta T_p \omega_r$) was zero. Equation (3) becames, $T_{M1} = T_M$. The test was repeated and the average value of T_M was calculated. $T_M(average) = .00083\ N.m/rad$.

The following relation gives the viscous damping coefficient of rotor about spin axis.

$$D_r = \frac{T_M(average)}{\omega_r} \tag{15}$$

And the following relations give the magnetic torque damping.

$$\delta T_p(\max) = \frac{T_{M1}(\max) - T_M(average)}{\omega_r} \tag{16a}$$

$$\delta T_p(\min) = \frac{T_{M1}(\min) - T_M(average)}{\omega_r} \tag{16b}$$

The obtained value are $\delta T_p(\max) = 4.7\times10^{-7}\ N.m/rad/s$ and

$\delta T_p(\min) = -2.6\times10^{-7}\ N.m/rad/s$; where used values are taken

$\delta T_p = \pm 4.7\times10^{-7}\ N.m/rad/s$

Substituting by the value of T_{M1} into equation (13), gives the pendulosity

$p = -0.0000115\ kg.m$

5. DETERMINATION OF THE ROTOR-RESPONSE DUE TO THE PENDULOSITY

The rotor was run up, and then it was offset in ϕ angle (horizontally). The precession and the spin coils were opened, then the pitch and yaw angles were recorded during a time interval 8 sec , Fig.12. The experiment conditions are summarized as follow:

a) $\dot{\gamma}_x = \dot{\gamma}_y = \dot{\gamma}_z = a_x = a_y = 0$

b) $T_p = 0$

c) $T_M = 0$

d) $a_z = -g$

Substitute these conditions into equation (1a), it results in:

$$pg - D_1\dot{\theta} - K\theta = I\ddot{\theta} + H\dot{\phi} \tag{17}$$

Substituting by $\dot{\theta}$, $\ddot{\theta}$, and $\dot{\phi}$ values into equation (17) at time t_1 and t_2 it results in:

The viscous damping about the gimbal axes (mechanical viscous damping) pluses the magnetic damping torque; $D_1 = 0.0011$ N.m/rad/s and the mechanical spring rate about the gimbal axes (direct-axis spring rate); $K = 0.00028$ N.m/rad . Substituting by δT_p and D_1 values into equation (2), it results in: The viscous damping about the gimbal axes $D = 0.0011$ N.m/rad/s

6. DETERMINATION OF THE ROTOR-RESPONSE DUE TO A GIVEN FINITE INPUT

The infrared source is mounted on a carrier, which moves by a constant speed (4.3 cm/s). The carrier is adjusted to move in a vertical plane at a distance L = 286 cm from the center of support (CS) of gyro gimbals. The data was taken for a positive displacement of the infrared source on the yaw direction as shown in Fig.13. The test conditions are summarized as follow:

a) $\dot{\gamma}_x = \dot{\gamma}_y = \dot{\gamma}_z = a_x = a_y = 0$

b) $E_1 = 0$

c) $E_2 = -1$

d) $a_z = -g$

Substitute these conditions into equation (1a), it results in:

$$T_P - \phi T_{M1} - D\dot{\theta} - K\theta + pg = I\ddot{\theta} + H\dot{\phi} \quad (18)$$

Substituting by $\theta, \dot{\theta}$, $\ddot{\theta}$, ϕ, and $\dot{\phi}$ values into equations (18), gives the precession torque $T_P = 0.000529\ N.m$

7. EFFECT OF MODELING PARAMETERS ON THE SYSTEM RESPONSE

The numerical solution of the seeker dynamical equations is introduced by Matlab/Simulink program, Fig.14, [12, 13]. The solution is based on the values of the parameters that are experimentally determined. The results of the experimental work are compared along with the numerical solution[9]. The results of the numerical solutions of the equations with changing the modeling parameters are introduced to predict the system response in each case, Fig.15-18.

8. RESULTS AND DISCUSSION

The Cross-axis spring rate (T_M), (spin motor torque constant) has an approximate value 0.00103 N.m/rad. The tracking capability of this type of the IR-seeker decreased with the existence of the spin motor torque due to the cross coupling between axes, Fig.15.

The Viscous damping coefficient of rotor about spin axis (D_r), (viscous drag on the rotor about its spin axis) has an approximate value 1.74×10^{-6} N.m/rad/s.

The Magnetic torque damping (δT_p), (precession torque due to induced current) has

an approximate value ± 4.7×10^{-7} N.m/rad/s. this torque can be neglected when it is compared with the viscous damping about the gimbal axes (D), (mechanical viscous damping).

The Mechanical viscous damping (D) has an approximate value 0.0011 N.m/rad/s. It has a low value in this type of IR–Seeker, Fig.16.

The Direct axis spring rate (K) has an approximate value 0.00028 N.m/rad. The values of the mechanical spring rate (K), Fig.17 , might be increased under the effect of any magnetic or electromagnetic torques, which are also directly proportional to gimbal displacement from a null position with respect to the case. The exposure of these types of gyro stabilized seekers to a magnetic field leads to the changing in the value of direct axis spring rate which hinders the process of tracking. Also, the continuation of the hindrance misleads the missile hence the head seeker should be electromagnetically isolated.

The Pendulous unbalance along spin axis (P) for our case study has an approximate value (-0.0000115) Kg.m.

The determination of the precession torque is an essential step in studying the seeker tracking capabilities. Thus, the required torque to realize a certain tracking rate can be estimated. Important relations can be developed between the precession torque, the precession current and the precession coil design parameters (windings number, wire diameter, and coil diameter). These relations are basic information in the coil design procedure. From the development point of view, the previous relations are used to estimate the electronic circuitry design that might be needed to achieve better tracking capabilities.

Based on the above measured dynamic parameter the relative magnitudes of the different dynamic error sources can be calculated. The prediction of the system response based on real values of the equations parameters can be considered as an essential step to any future development in the seeker system, which can be modified or reconstructed using more advanced techniques.

9. CONCLUSIONS

1- The gyro angular momentum is the dominant term in the gyro torque equation. The unbalance torque due to the pendulous unbalance and the spin motor torque represents the dominant undesired torques (gimbal torques) in the gyro torque equation. The determination of the pendulous unbalance along spin axis will introduce an additional test for the IR–seeker test procedures in a way to confirm the allowable range of pendulous after repair processes.

2- The tracking capability of this type of the IR-seeker decreases with the existence of the spin motor torque due to the cross coupling between axes. Since the cross coupling cannot be totally eliminated, the recent trends are concentrated towards the design of new kinds of seeker gyroscopes that have a reduced cross coupling between rotor spin and precession.

3- The effect of the magnetic torque damping (precession torque due to induced current) can be neglected when it is compared with the viscous damping about the gimbal axes (mechanical viscous damping) which can also be neglected in this type of IR–seeker.

REFERENCES

[1] Ronald N. Arnold and Leonard Maunder “Gyrodynamics and Its Engineering Applications”, Academic Press New York and London, 1961.

[2] Paull H. Savet, “Gyroscopes: Theory and Design”, McGraw-Hill Book Company, Inc., 1961.

[3] Manuel Fernandez and George R. Macomber “Inertial Guidance Engineering”, Prentice-Hall, Inc., 1962.

[4] J. B. Scarborough, “The Gyroscope Theory and Applications”, Inter-science publishers, London, 1958.

[5] E. Russell Johnston, Jr. and Ferdinand P. Beer “Vector Mechanics for Engineering”, McGraw-Hill, Inc., 1977.

[6] S. A. White, “Dynamics of Solenoidal-Torqued Gyro-Stablized Seeker Assembly for Guidance and Tracking”, IEEE Trans. Aerospace and electronics systems, vol. AES-2, No. 10, pp. 113-122, Jan. 1974.

[7] Ahmed A. Shabana, “Dynamics of Multibody Systems”, John wiley & Sons, 1989.

[8] T. J. Chumg “Continuum Mechanics”, Prentice Hall, Englewood Cliffs, New Jersey, 1988.

[9] Ali A. A., “Performance Evaluation of a Gyro-Stabilized Platform”, M.Sc. Thesis, M. T. C., Cairo, March 2005.

[10] Technical manual of IR-seeker assembly

[11] Fredrick W. Hughes, “Op Amp Handbook”, Prentice Hall, Inc., New Jersey, 1981.

[12] Brain R. Hunt, Ronald L.Lipsan, Jonathan M. Rosenberg, “A Guide to MATLAB for Beginners and Experienced Users”, John Wiley and Sons, Inc., 2001.

[13] Kevin R. Coombes, Brian R. Hunt, Ronald L. Lipsman, “Differential Equations with MATLAB”, John Wiley and Sons, Inc., 2000.

[14] Allan Dushman, “On Gyro Drift Models and Their Evaluation”, IRE Trans. on Aerospace and Navigational Electronics, Dec. 1962.

[15] E. J. Eichblatt, Jr. and A. Pgnataro, “Test and Evaluation of the Tactical Missile”, Ed. Emil J. Eichblatt, Jr., Pacific missile test center, California, Library of congress, 1989.

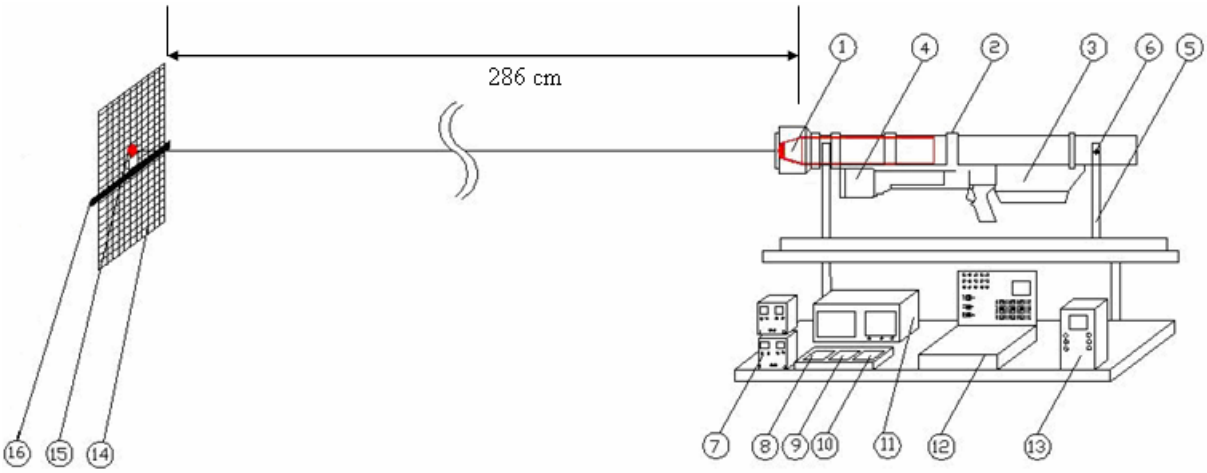

1. Heat seeking missile
2. Launcher
3. Gripstock
4. Power plug
5. The fixture
6. Fixation bolt
7. Two Power supplies
8. Amplifier circuit
9. Integrator circuit
10. Filter circuit
11. Digitizing oscilloscope
12. Analog computer
13. Power supply
14. Vertical plane board
15. Infrared source
16. Movable carrier

Fig.1. Schematic diagram of the test rig, the missile system, and the experimental setup devices, which used in offset and reference frame initial adjustment

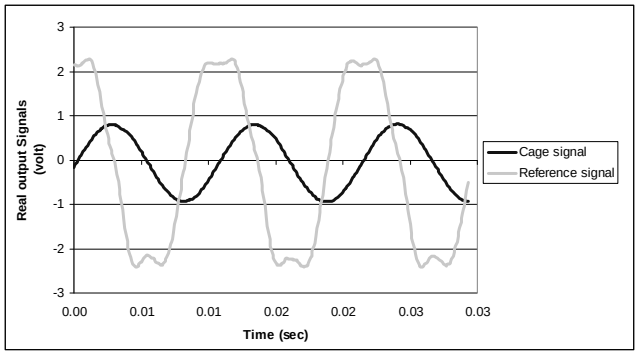

Fig.2. Reference and cage signals, general position

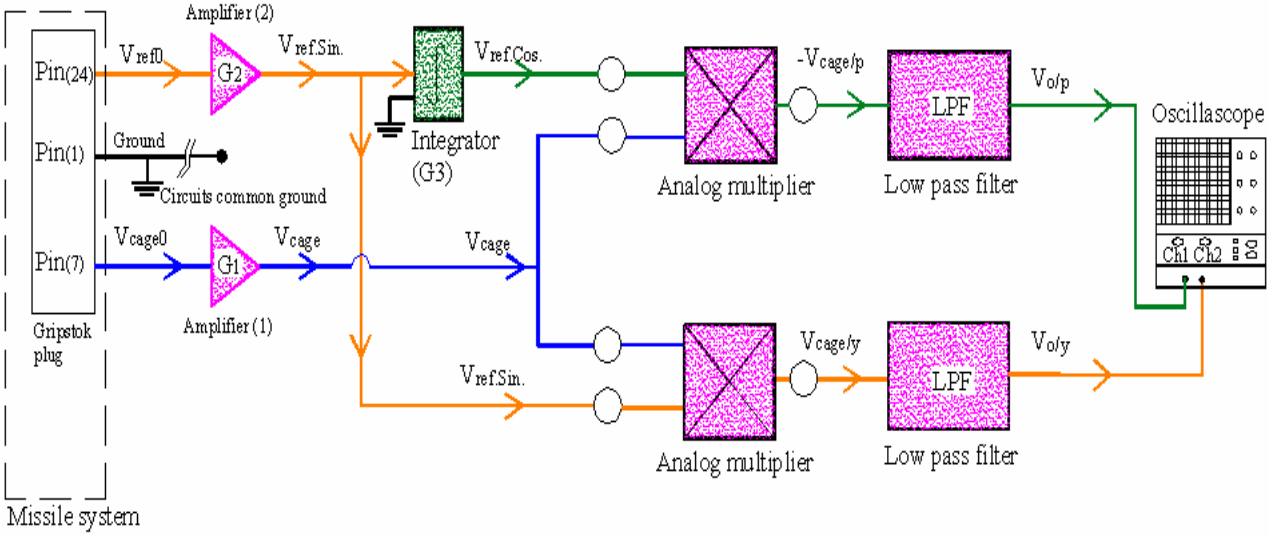

Fig.3. Block diagram of the separation process of the yaw and pitch components of the cage coil signal, offset and reference frame initial adjustment

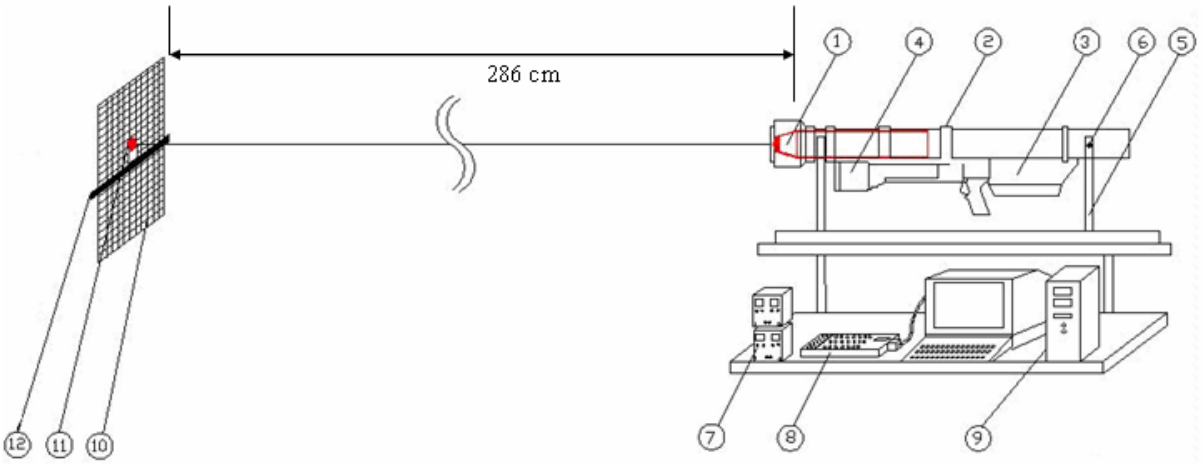

1. Heat seeking missile
2. Launcher
3. Gripstock
4. Power plug
5. The fixture
6. Fixation bolt
7. Two Power supplies
8. Data Acquisitions terminal
9. PC-computer
10. Vertical plane board
11. Infrared source
12. Movable carrier

Fig.4. Schematic diagram of the test rig, the missile system, and the experimental setup devices, which used in offset and reference frame fine adjustment

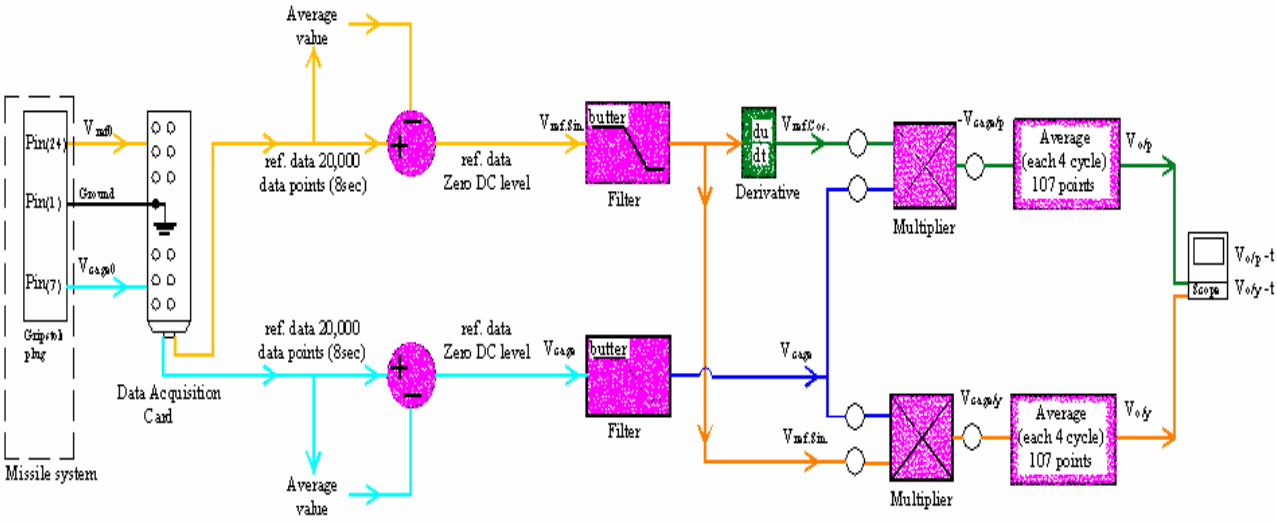

Fig.5. Block diagram of the separation process of the yaw and pitch components of the cage coil signal, offset and reference frame fine adjustment

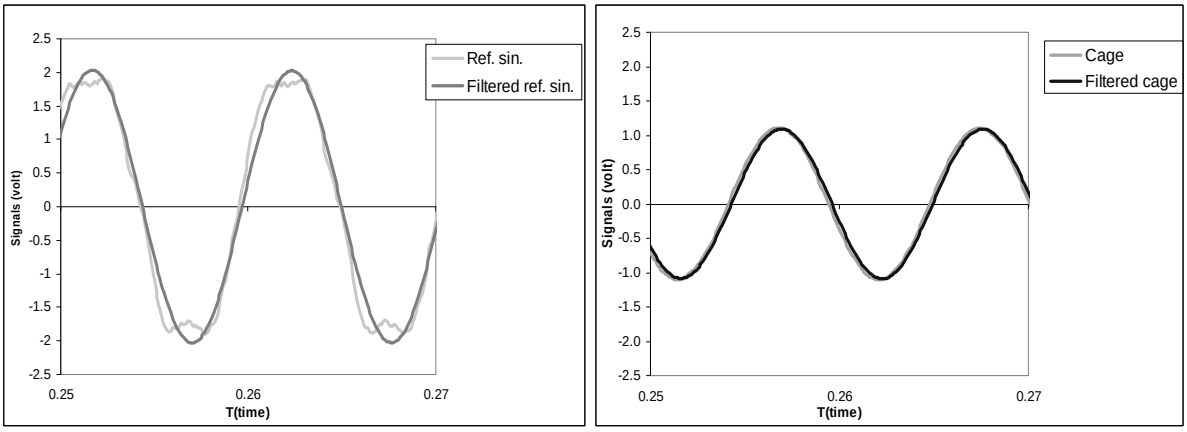

a)Reference signal b)Cage sighal

Fig.6. Filtered signals

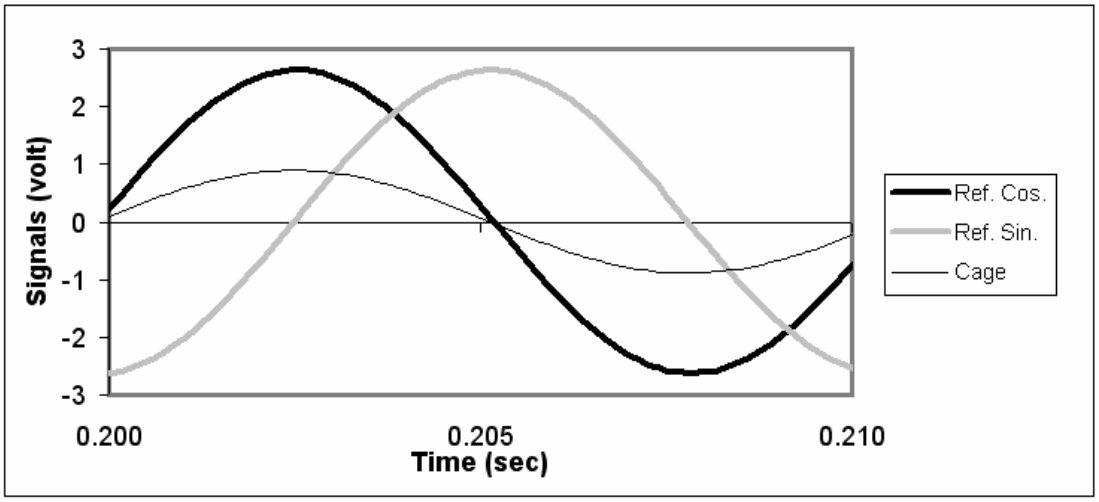

a) Ref. Sin., Ref. Cos. , and Cage signal(Multipliers inputs)

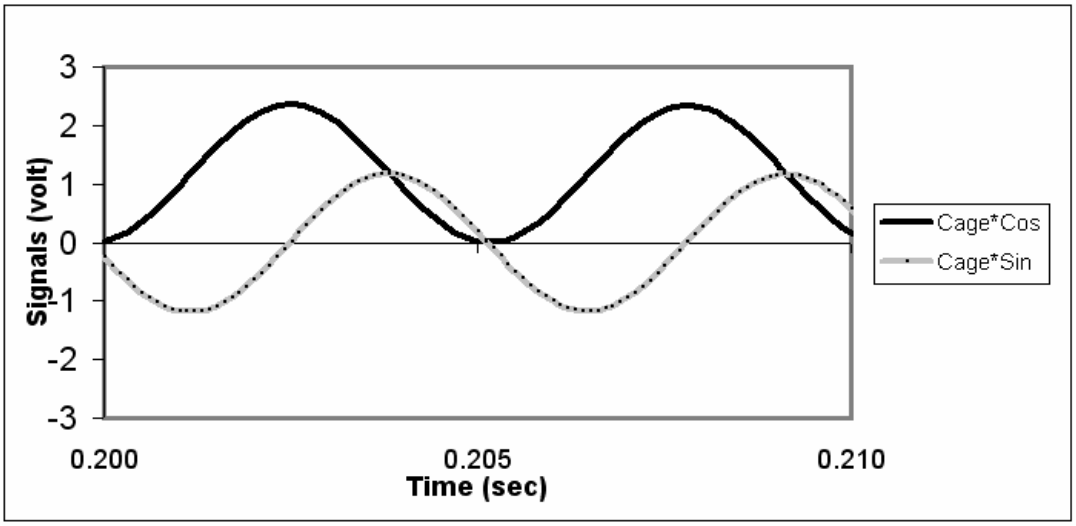

b) $V_{cage/p}$ and $V_{cage/y}$ (Multipliers outputs)

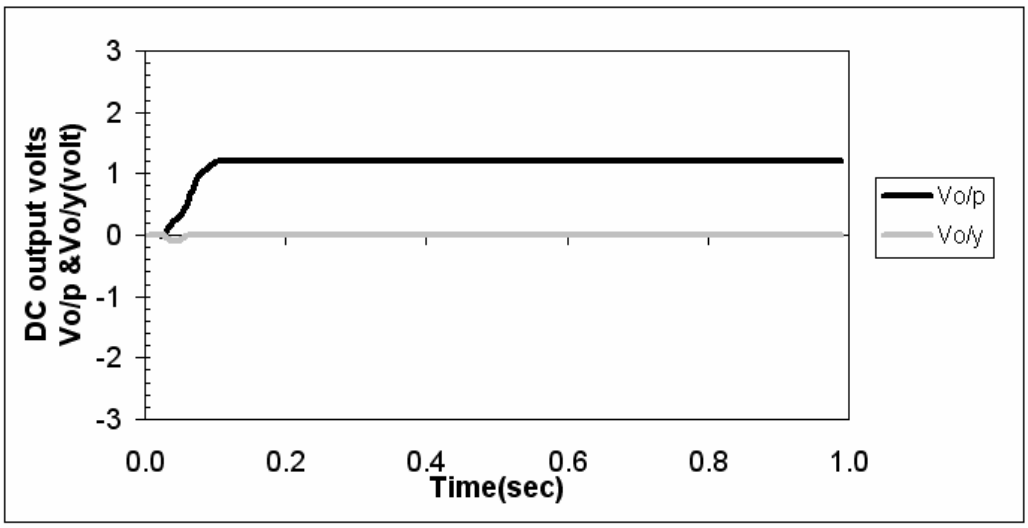

c) $V_{o/p}$ and $V_{o/y}$, (DC output volts)

Fig.7. Multipliers signals

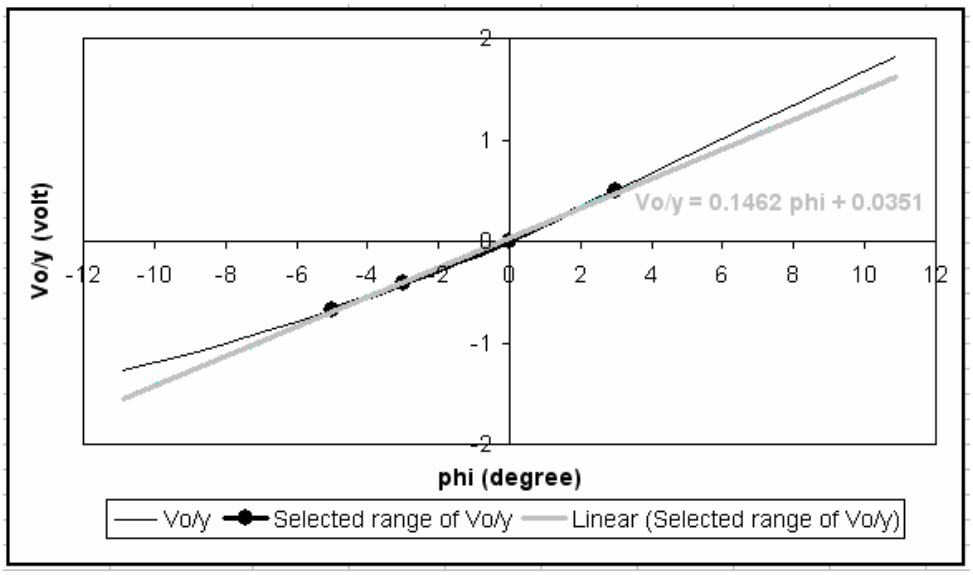

Fig.8. Calibration curve in the yaw direction (position 1)

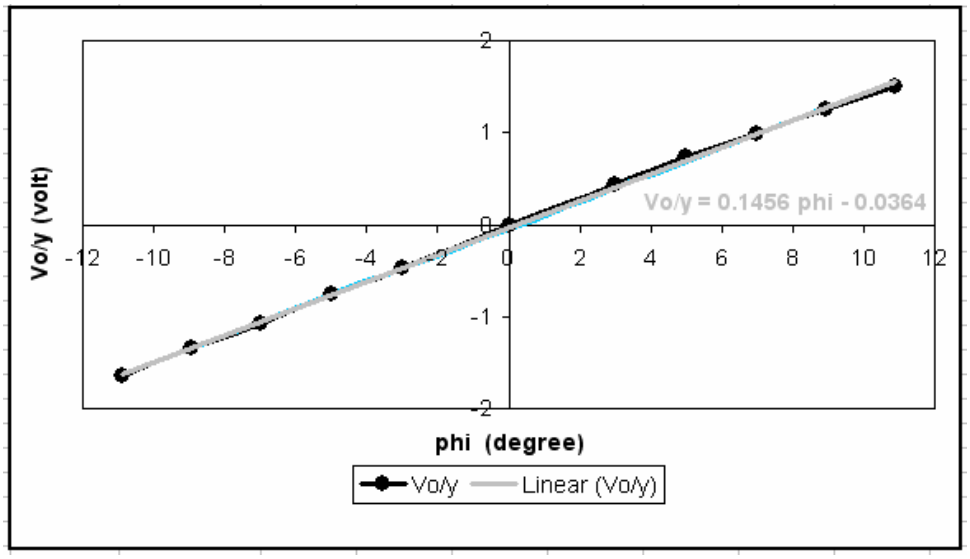

Fig.9. Calibration curve in the yaw direction (position 2)

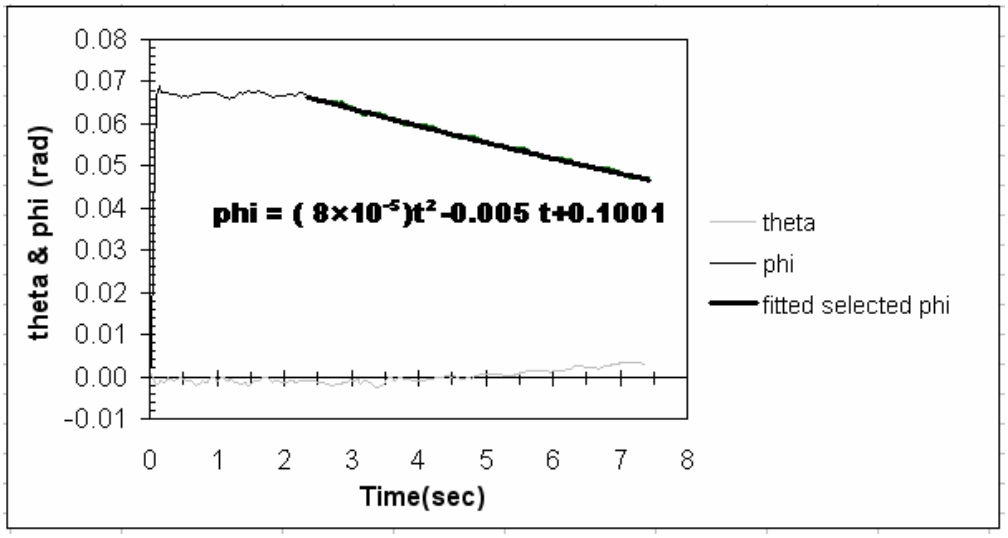

Fig.10. pitch and yaw angles, No error signal

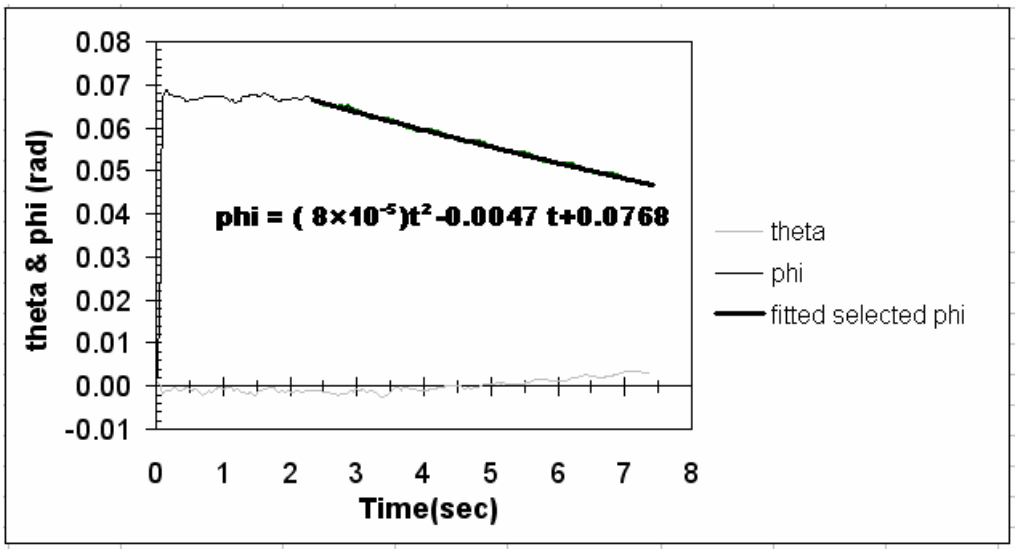

Fig.11. pitch and yaw angles, precession coils opened

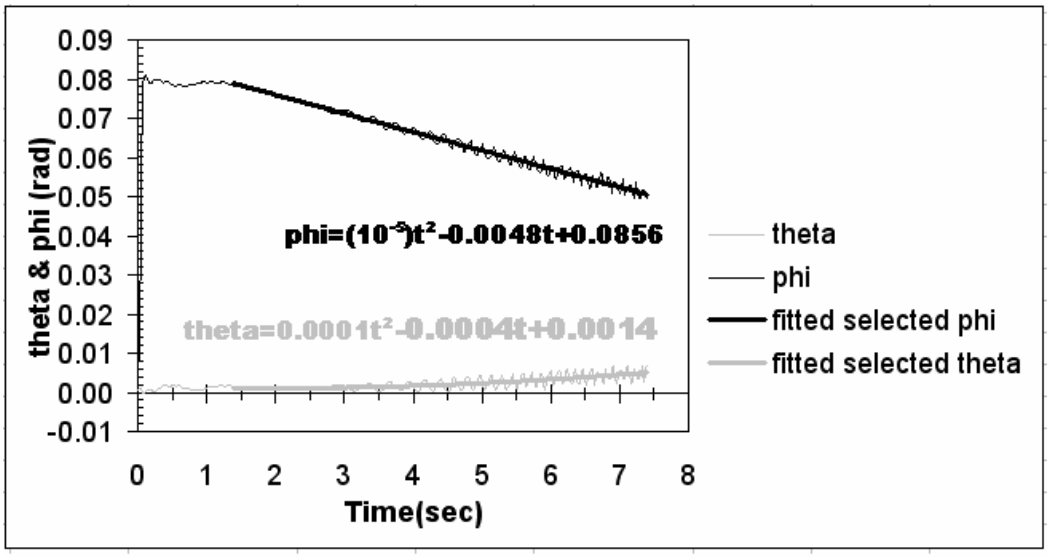

Fig.12. Pitch and Yaw angles precession and spin coils opened

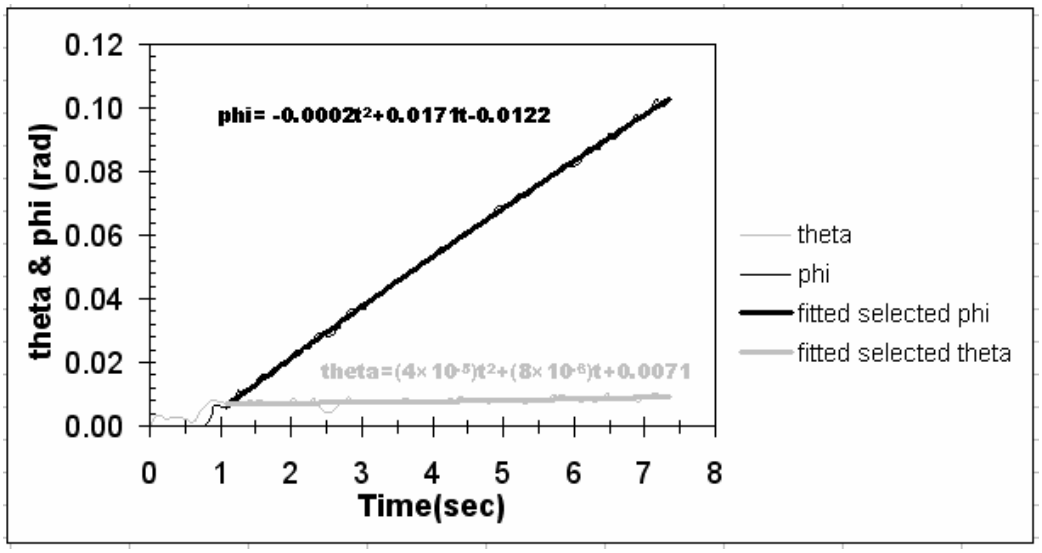

Fig.13. Gyro response to an infrared source moving with a constant speed

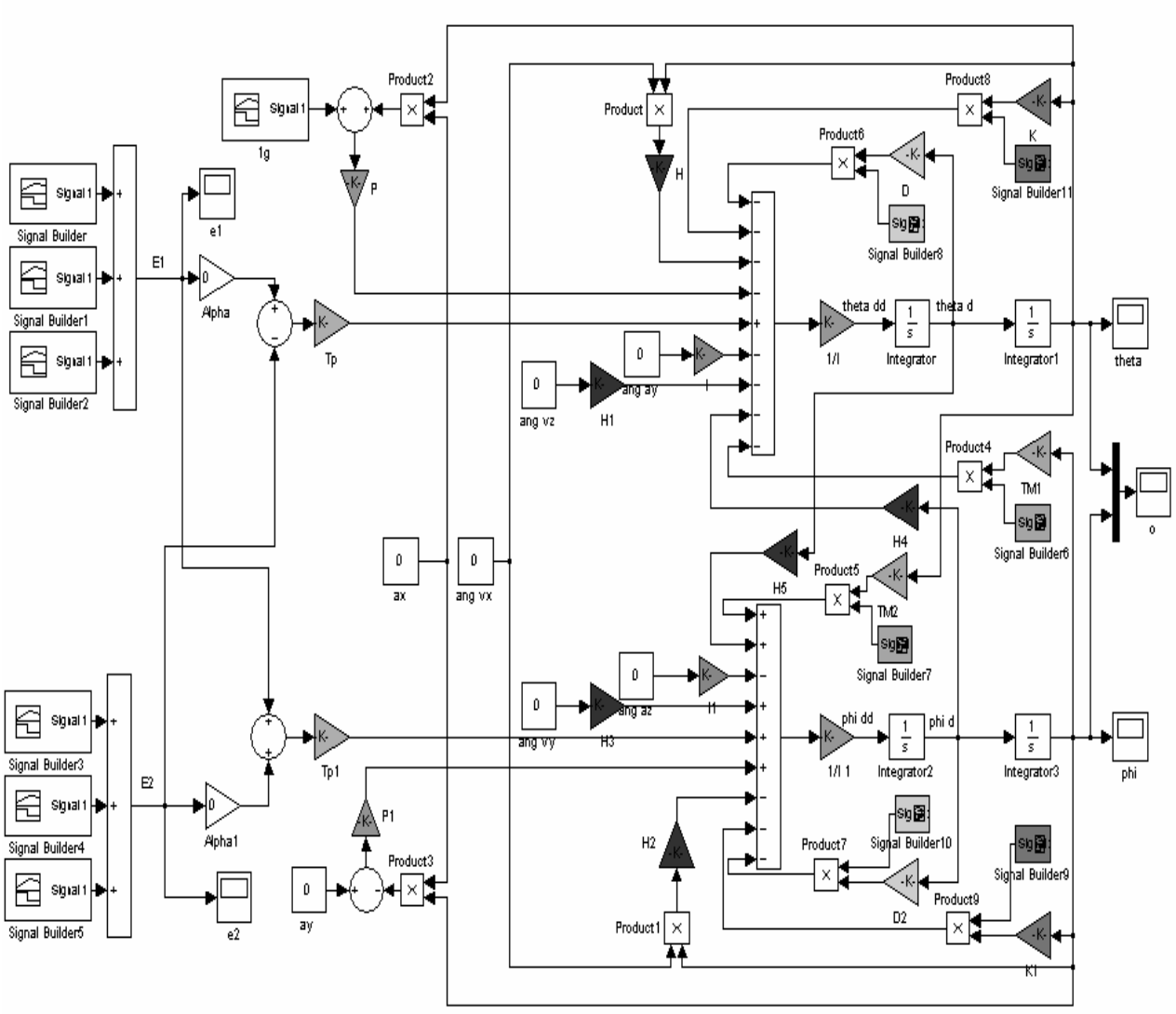

Fig.14. Simulink detailed block diagram

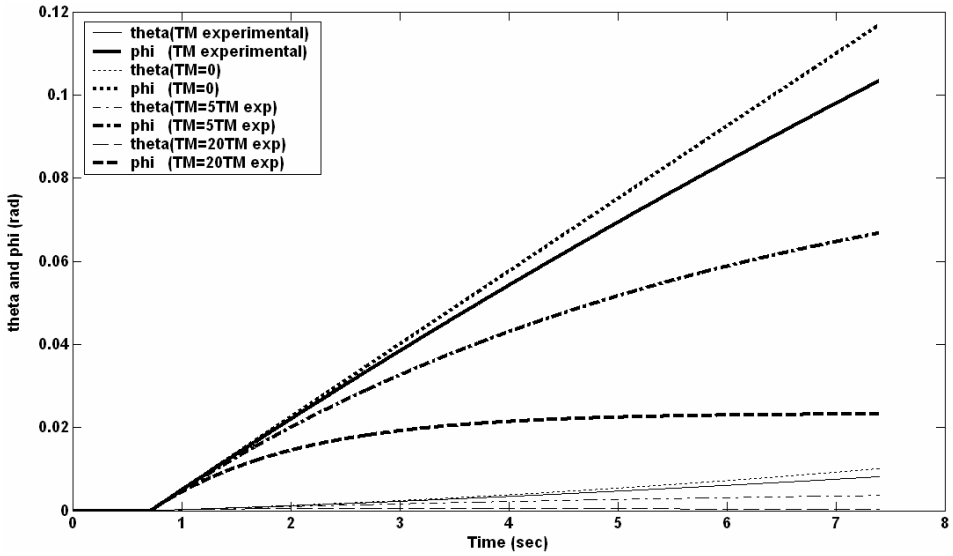

Fig.15. Effect of spin motor torque (TM) on the system response for a step input

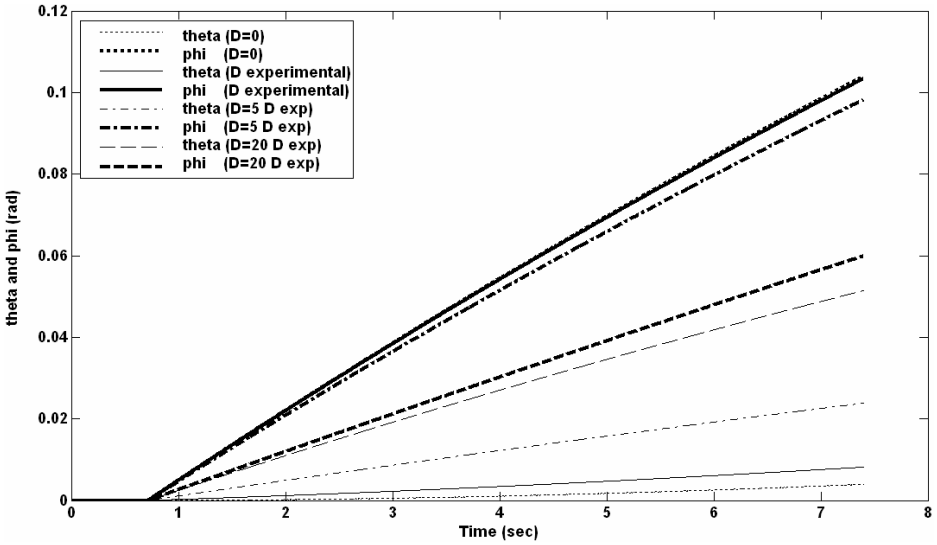

Fig.16. Effect of viscous damping (D) on the system response for a step input

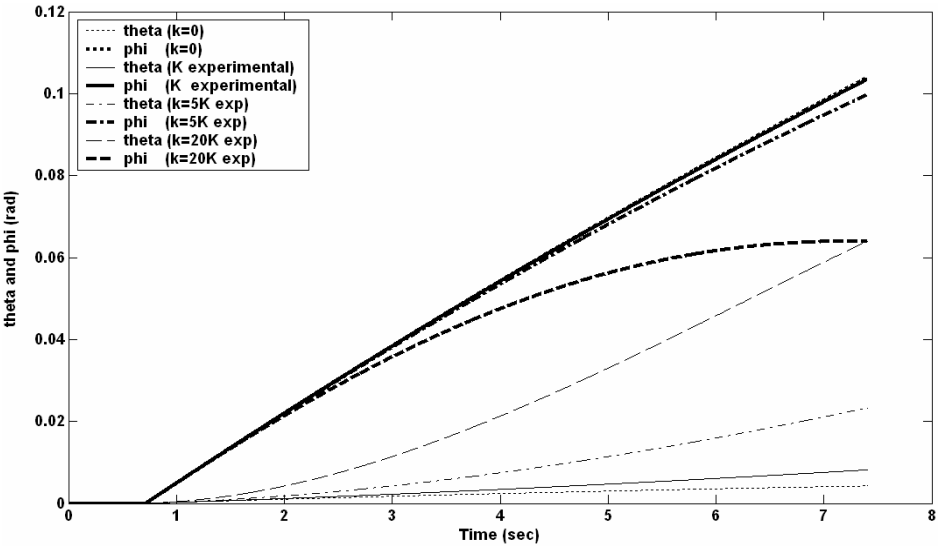

Fig.17. Effect of direct-axis spring rate (K) on the system response for a step input

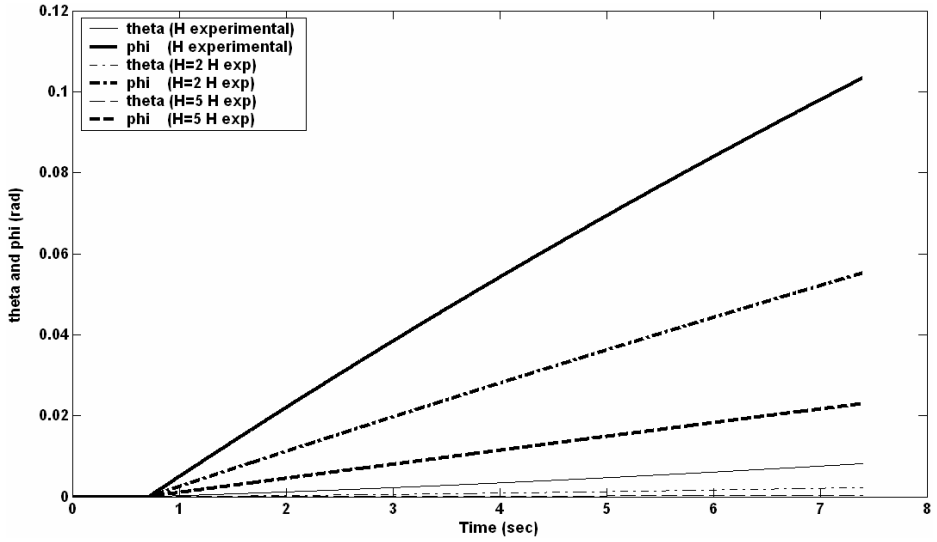

Fig.18. Effect of angular momentum (H) on the system response for a step input